is structurally similar to the CpRu(coumarin-6)$^+$ system in that the Cp*Ru$^+$ groups are not bound to the main π system of the highly fluorescent rubrene group but rather to electron-withdrawing substituent groups. In this case as well, complexation of the rubrene caused a significant red shift in both the absorption and emission maxima.

Acknowledgment. R.S.K. acknowledges support from the Marshall H. and Nellie Alworth Memorial Fund. This material is based upon work supported in part by the National Science Foundation under Grant No. CHE-8722843.

Registry No. [CpRu(coum-1)]PF_6, 120546-44-3; [CpRu(coum-2)]-PF_6, 120546-46-5; [CpRu(coum-311)]PF_6, 120546-48-7; [CpRu(coum-334)]PF_6, 120546-50-1; [CpRu(coum-338)]PF_6, 120546-52-3; [CpRu-(coum-6)]PF_6, 120546-54-5; [CpRu$(CH_3CN)_3$]PF_6, 80049-61-2; coumarin-1, 91-44-1; coumarin-2, 26078-25-1; coumarin-311, 87-01-4; coumarin-334, 55804-67-6; coumarin-338, 62669-75-4; coumarin-6, 38215-36-0.

Contribution from Exxon Research and Engineering Company, Clinton Township, Route 22 East, Annandale, New Jersey 08801, and Department of Chemistry, University of Minnesota, Minneapolis, Minnesota 55455

Comparison of the Electronic Structures of Homo- and Heteronuclear Butterfly Clusters Containing Carbide, Nitride, and Oxide Ligands. Crystal and Molecular Structure of [PPN][$Ru_4N(CO)_{12}$]

Suzanne Harris,*[†] Margaret L. Blohm,[‡] and Wayne L. Gladfelter*[‡]

Received November 2, 1988

The electronic structures of several butterfly clusters containing carbon, nitrogen, and oxygen atoms have been studied by using Fenske–Hall molecular orbital calculations. Comparison of the calculated electronic structures of $[Fe_4X(CO)_{12}]^{n-}$ (X = C, N, O) shows that the major effect of substituting the smaller N and O atoms is a weakening of the X–wingtip Fe bond. These results suggest that the O–Fe interactions may not be strong enough to maintain the same butterfly cluster geometry as that observed for $[Fe_4C(CO)_{12}]^{2-}$ and $[Fe_4N(CO)_{12}]^-$. The coordinates for the homonuclear ruthenium nitride cluster were obtained from the single-crystal X-ray crystallographic analysis of [PPN][$Ru_4N(CO)_{12}$] [$P\bar{1}$ space group, a = 10.815 (2) Å, b = 14.185 (2) Å, c = 16.433 (9) Å, α = 91.98 (3)°, β = 94.68 (3)°, γ = 97.79 (2)°, Z = 2], which established that it was isomorphous with the tetrairon nitrido cluster. The major difference between the electronic structure of $[Fe_4N(CO)_{12}]^-$ and that of $[Ru_4N(CO)_{12}]^-$ is the stronger metal–metal bonding in the Ru_4N cluster. Calculations for the two isomers of $[FeRu_3N(CO)_{12}]^-$ show that substitution of Fe into the Ru_4 framework of $[Ru_4N(CO)_{12}]^-$ results in relatively small perturbations of the electronic structure of the cluster.

Introduction

The so-called butterfly structure found in many four-metal-atom clusters is capable of binding a wide variety of substrates. Among the more actively studied compounds are those containing a single main-group atom such as C,[1] N,[2] and O.[3] Much of the effort in studying the structure and reactivity of these atoms exposed along the edge of a cluster stems from the interest in comparing them to surface-coordinated atoms.[4] The availability of such a set of isoelectronic and isostructural compounds makes them attractive subjects for detailed comparisons of the bonding.

Previous studies on the electronic structure of butterfly clusters containing carbide and related carbon-bound ligands have established the basic patterns of the orbital interactions and their relative energies.[5-7] In the study presented here we consider the changes affected first by moving from carbide to nitride and oxide ligands and then by replacing a 3d metal (Fe) with a 4d metal (Ru). We first compare the electronic structures of $[Fe_4C(CO)_{12}]^{2-}$, $[Fe_4N(CO)_{12}]^-$, and the model cluster $Fe_4O(CO)_{12}$. This is followed by a description of the molecular structure of [PPN][$Ru_4N(CO)_{12}$] and a comparison of the electronic structures of $[Ru_4N(CO)_{12}]^-$ and $[Fe_4N(CO)_{12}]^-$. Finally, the electronic structure of the heterometallic cluster $[FeRu_3N(CO)_{12}]^-$ is discussed.

Experimental Section

X-ray Crystallographic Study. Orange crystals of [PPN][$Ru_4N(CO)_{12}$][8] were grown from an ether/hexane solution. Details of the structural analysis (Table I) are similar to those of closely related compounds studied in our laboratory.[9] A preliminary peak search indicated the crystal was triclinic, and the $P\bar{1}$ space group was chosen. The cell data were very similar to those found for the analogous iron cluster,[10] suggesting that they were isomorphous. The Ru structure was solved by using the coordinates from the Fe structure. All atoms in the cluster and the P and N atoms of the cation were refined with the use of anisotropic temperature factors. The hydrogen atom positions were calculated and

Table I. Summary of Crystallographic Data

Crystal Parameters	
cryst syst	triclinic
space group	$P\bar{1}$
formula	$C_{48}H_{30}N_2P_2O_{12}Ru_4$
fw	1293.0
a, Å	10.815 (2)
b, Å	14.185 (2)
c, Å	16.433 (9)
α, deg	91.98 (3)
β, deg	94.68 (3)
γ, deg	97.79 (2)
V, Å^3	2487 (2)
Z	2
ρ(calcd), g cm^{-3}	1.73
temp, °C	23
abs coeff, cm^{-1}	12.92
cryst dimens, mm	0.04 × 0.12 × 0.25
transmissn factors, max–min, %	100–85.9
abs cor applied	empirical (Ψ scans)
Measurement of Intensity Data	
diffractometer	Enraf-Nonius CAD-4
radiation	Mo Kα (λ = 0.710 73 Å)
monochromator	graphite cryst
programs used	Enraf-Nonius CAD-4-SDP programs
scan type	ω–2θ
scan range, deg	$0 \le 2\theta \le 48$
reflns measd	$+h,\pm k,\pm l$
no. of unique reflns	7787
no. of reflns used	5354
no. of variables	613
cutoff	2σ
p	0.03
extinction coeff	2.62 × 10^{-8}
R	0.031
R_w	0.033
error in observn of unit wt	1.131

[†] Exxon Research and Engineering Co.
[‡] University of Minnesota.

0020-1669/89/1328-2290$01.50/0

Table II. Positional Parameters for [PPN][$Ru_4N(CO)_{12}$]

atom	x	y	z	atom	x	y	z
Ru1	0.19234 (4)	0.28701 (3)	0.78429 (2)	C3A	0.5141 (5)	0.6366 (4)	1.0016 (3)
Ru2	0.08991 (4)	0.37964 (3)	0.66299 (2)	C4A	0.3961 (5)	0.6084 (4)	0.9659 (3)
Ru3	−0.06723 (4)	0.26935 (3)	0.76018 (3)	C5A	0.3713 (5)	0.6179 (4)	0.8837 (4)
Ru4	0.18761 (4)	0.21407 (3)	0.62353 (3)	C6A	0.4651 (5)	0.6546 (4)	0.8374 (3)
P1	0.7063 (1)	0.73239 (8)	0.81193 (7)	C1B	0.7065 (4)	0.6477 (3)	0.7284 (3)
P2	0.6022 (1)	0.90563 (8)	0.75353 (8)	C2B	0.7610 (5)	0.6785 (4)	0.6599 (3)
N2	0.6943 (4)	0.8351 (3)	0.7819 (2)	C3B	0.7646 (6)	0.6145 (4)	0.5943 (3)
N	0.0570 (3)	0.2378 (3)	0.6907 (2)	C4B	0.7143 (6)	0.5221 (4)	0.5985 (3)
O11	0.1596 (4)	0.4323 (3)	0.9185 (2)	C5B	0.6612 (6)	0.4902 (4)	0.6673 (4)
O12	0.2161 (5)	0.1124 (3)	0.8845 (3)	C6B	0.6597 (5)	0.5539 (4)	0.7324 (3)
O13	0.4683 (4)	0.3528 (3)	0.7709 (3)	C1C	0.8542 (4)	0.7408 (3)	0.8715 (3)
O21	0.0149 (4)	0.5510 (3)	0.7515 (3)	C2C	0.9202 (5)	0.8283 (4)	0.8968 (4)
O22	−0.0774 (4)	0.3859 (3)	0.5054 (2)	C3C	1.0339 (5)	0.8327 (4)	0.9423 (4)
O23	0.3307 (4)	0.4928 (3)	0.6171 (3)	C4C	1.0805 (5)	0.7525 (5)	0.9636 (4)
O31	−0.3148 (4)	0.2500 (3)	0.6587 (4)	C5C	1.0178 (5)	0.6661 (4)	0.9390 (3)
O32	−0.1112 (4)	0.0894 (3)	0.8540 (3)	C6C	0.9030 (5)	0.6585 (4)	0.8932 (3)
O33	−0.1568 (4)	0.4081 (3)	0.8816 (2)	C1D	0.4474 (5)	0.8499 (3)	0.7201 (3)
O41	0.0478 (4)	0.1698 (3)	0.4569 (2)	C2D	0.4303 (5)	0.7921 (4)	0.6487 (3)
O42	0.2403 (5)	0.0153 (3)	0.6573 (3)	C3D	0.3155 (6)	0.7416 (4)	0.6254 (4)
O43	0.4416 (4)	0.2809 (4)	0.5600 (3)	C4D	0.2172 (6)	0.7465 (4)	0.6715 (4)
C11	0.1691 (5)	0.3764 (4)	0.8682 (3)	C5D	0.2313 (5)	0.8020 (5)	0.7408 (4)
C12	0.2074 (5)	0.1764 (4)	0.8463 (4)	C6D	0.3466 (5)	0.8544 (4)	0.7666 (3)
C13	0.3637 (5)	0.3268 (4)	0.7734 (3)	C1E	0.5939 (4)	0.9922 (3)	0.8347 (3)
C21	0.0403 (5)	0.4845 (4)	0.7197 (3)	C2E	0.5521 (5)	1.0781 (4)	0.8200 (3)
C22	−0.0162 (5)	0.3836 (4)	0.5644 (3)	C3E	0.5547 (6)	1.1451 (4)	0.8840 (4)
C23	0.2408 (5)	0.4484 (4)	0.6330 (3)	C4E	0.5975 (5)	1.1260 (4)	0.9608 (3)
C31	−0.2223 (5)	0.2561 (4)	0.6963 (4)	C5E	0.6396 (5)	1.0421 (4)	0.9761 (3)
C32	−0.0992 (5)	0.1582 (4)	0.8203 (3)	C6E	0.6378 (4)	0.9756 (3)	0.9131 (3)
C33	−0.1240 (5)	0.3556 (4)	0.8374 (3)	C1F	0.6640 (5)	0.9686 (3)	0.6689 (3)
C41	0.1033 (5)	0.1859 (4)	0.5181 (3)	C2F	0.5867 (5)	1.0120 (4)	0.6156 (3)
C42	0.2236 (6)	0.0909 (4)	0.6442 (4)	C3F	0.6382 (6)	1.0637 (4)	0.5540 (4)
C43	0.3478 (5)	0.2545 (4)	0.5836 (4)	C4F	0.7630 (6)	1.0711 (4)	0.5447 (4)
C1A	0.5860 (4)	0.6832 (3)	0.8737 (3)	C5F	0.8404 (6)	1.0283 (4)	0.5978 (4)
C2A	0.6087 (5)	0.6747 (4)	0.9570 (3)	C6F	0.7902 (5)	0.9765 (4)	0.6603 (3)

Table III. Bond Distances (Å) in [PPN][$Ru_4N(CO)_{12}$]

Ru1–Ru2	2.672 (1)	Ru3–C32	1.897 (6)
Ru1–Ru3	2.779 (1)	Ru3–C33	1.925 (6)
Ru1–Ru4	2.798 (1)	Ru4–C41	1.894 (6)
Ru2–Ru3	2.789 (1)	Ru4–C42	1.877 (6)
Ru2–Ru4	2.781 (1)	Ru4–C43	1.925 (6)
Ru3–Ru4	3.838 (1)	C11–O11	1.146 (6)
N–Ru1	2.069 (3)	C12–O12	1.132 (6)
N–Ru2	2.069 (3)	C13–O13	1.146 (6)
N–Ru3	1.921 (3)	C21–O21	1.140 (5)
N–Ru4	1.919 (3)	C22–O22	1.133 (5)
Ru1–C11	1.896 (6)	C23–O23	1.139 (6)
Ru1–C12	1.917 (6)	C31–O31	1.124 (6)
Ru1–C13	1.888 (6)	C32–O32	1.135 (6)
Ru2–C21	1.889 (5)	C33–O33	1.134 (5)
Ru2–C22	1.914 (5)	C41–O41	1.129 (6)
Ru2–C23	1.895 (6)	C42–O42	1.137 (6)
Ru3–C31	1.887 (6)	C43–O43	1.136 (6)
P1–N2	1.573 (4)	P1–C (av)	1.794 (4)
P2–N7	1.561 (4)	P2–C (av)	1.796 (5)
C–C (av)	1.38 (3)		

Table IV. Selected Bond Angles (deg) in [PPN][$Ru_4N(CO)_{12}$]

Ru2–Ru1–Ru4	61.06 (2)	Ru2–Ru3–C32	148.7 (2)
Ru3–Ru1–Ru4	86.98 (2)	Ru2–Ru3–C33	107.0 (2)
Ru2–Ru1–N	49.76 (9)	N–Ru3–C31	107.7 (2)
Ru3–Ru1–N	43.7 (1)	N–Ru3–C32	102.8 (2)
Ru2–Ru1–C11	95.2 (2)	N–Ru3–C33	150.3 (2)
Ru2–Ru1–C12	153.2 (2)	C31–Ru3–C32	97.6 (2)
Ru2–Ru1–C13	99.9 (2)	C31–Ru3–C33	91.5 (2)
Ru3–Ru1–C11	82.9 (2)	C32–Ru3–C33	96.7 (2)
Ru3–Ru1–C12	99.0 (2)	Ru1–N–Ru2	80.5 (1)
Ru3–Ru1–C13	161.4 (2)	Ru1–N–Ru3	88.2 (1)
Ru4–Ru1–C11	156.2 (2)	Ru1–N–Ru4	89.0 (1)
Ru4–Ru1–C12	102.2 (2)	Ru2–N–Ru3	88.7 (1)
Ru4–Ru1–C13	84.6 (2)	Ru2–N–Ru4	88.3 (1)
N–Ru1–C11	123.74 (2)	Ru3–N–Ru4	176.2 (2)
N–Ru1–C12	103.5 (2)	Ru1–C11–O11	177.3 (5)
N–Ru1–C13	126.2 (2)	Ru1–C12–O12	178.4 (6)
C11–Ru1–C12	100.7 (2)	Ru1–C13–O13	176.5 (5)
C11–Ru1–C13	98.5 (2)	Ru2–C21–O21	176.1 (5)
C12–Ru1–C13	99.0 (2)	Ru2–C22–O22	178.9 (5)
Ru1–Ru3–Ru2	57.36 (1)	Ru2–C23–O23	177.1 (5)
Ru1–Ru3–N	48.1 (1)	Ru3–C31–O31	178.7 (5)
Ru1–Ru3–C31	154.5 (2)	Ru3–C32–O32	175.1 (5)
Ru1–Ru3–C32	96.2 (2)	Ru3–C33–O33	178.4 (5)
Ru1–Ru3–C33	108.1 (2)	Ru4–C41–O41	176.6 (5)
Ru2–Ru3–C31	102.0 (2)	Ru4–C42–O42	177.2 (7)
Ru4–C43–O43	178.1 (6)		
P1–N2–P2	145.6 (3)	C–P1–N2 (av)	111 (4)
C–P1–C (av)	107 (1)	C–P2–N2 (av)	111 (3)
C–P2–C (av)	108 (1)	C–C–C (av)	120 (2)

their contributions added to the refinement, but their positions and temperature factors were not refined. The final difference Fourier map indicated no significant features. The values of the atomic scattering factors used in the calculations were taken from the usual tabulation,[11] and the effects of anomalous dispersion were included for the non-hydrogen atoms. The positional parameters, bond distances, and bond angles are listed in Tables II–IV, respectively.

(1) Bradley, J. S. *Adv. Organomet. Chem.* **1985**, *22*, 1.
(2) Gladfelter, W. L. *Adv. Organomet. Chem.* **1985**, *24*, 41.
(3) Schauer, C. K.; Shriver, D. F. *Angew. Chem., Int. Ed. Engl.* **1987**, *26*, 255.
(4) Muetterties, E. L.; Rhodin, T. N.; Bard, E.; Brucker, C. F.; Pretzer, W. R. *Chem. Rev.* **1979**, *79*, 91.
(5) Housecroft, C. E.; Fehlner, T. P. *Organometallics* **1983**, *2*, 690. Fehlner, T. P.; Housecroft, C. E. *Organometallics* **1984**, *3*, 764.
(6) Wijeyesekera, S. D.; Hoffmann, R.; Wilder, C. N. *Organometallics* **1984**, *3*, 962.
(7) Harris, S.; Bradley, J. S. *Organometallics* **1984**, *3*, 1086.
(8) Blohm, M. L.; Gladfelter, W. L. *Organometallics* **1985**, *4*, 45.
(9) Fjare, D. E.; Gladfelter, W. L. *J. Am. Chem. Soc.* **1984**, *106*, 4799.
(10) Fjare, D. E.; Gladfelter, W. L. *Inorg. Chem.* **1981**, *20*, 3533.
(11) (a) Cromer, D. T.; Waber, J. T. *International Tables for X-ray Crystallography*; Kynoch: Birmingham, England, 1974; Vol. IV, Table 2.2A. Cromer, D. T. *Ibid.*, Table 2.3.1. (b) Cromer, D. T.; Ibers, J. A. *Ibid.*, Table 2.2C.

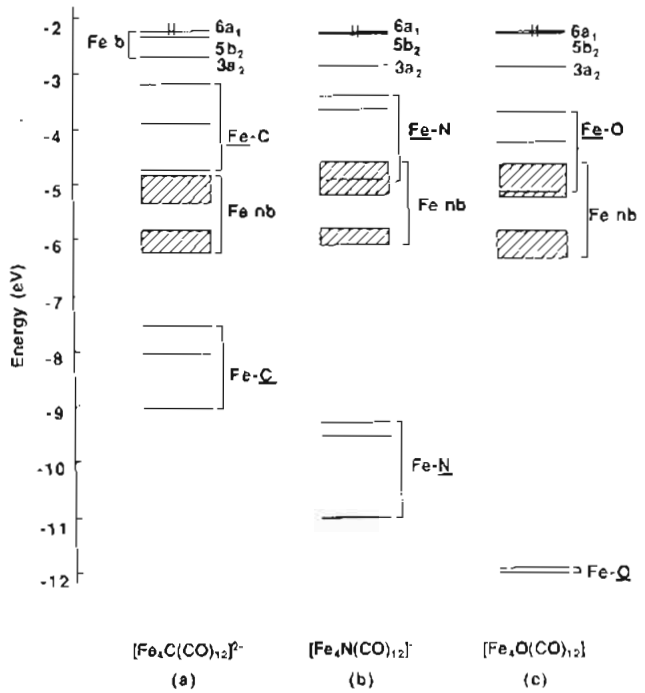

Figure 1. Calculated energy level diagrams for (a) $[Fe_4C(CO)_{12}]^{2-}$, (b) $[Fe_4N(CO)_{12}]^-$, and (c) $Fe_4O(CO)_{12}$. The energy scale corresponds to the energies calculated for $[Fe_4N(CO)_{12}]^-$. For comparison, the energies of the levels in the other clusters have been scaled so that the HOMO lies at the same energy in all three clusters.

Calculational Details Molecular orbital calculations were carried out for $[Fe_4N(CO)_{12}]^-$, $[Ru_4N(CO)_{12}]^-$, $[FeRu_3N(CO)_{12}]^-$, and the model cluster $Fe_4O(CO)_{12}$. Calculations for $[Fe_4C(CO)_{12}]^{2-}$ have been reported previously,[7] and the results of those calculations are used for comparison here. The structures of $[Fe_4N(CO)_{12}]^-$[10] and $[FeRu_3N(CO)_{12}]^-$[9] were reported earlier, and the structure of $[Ru_4N(CO)_{12}]^-$ is reported here. Calculations were carried out for these clusters in both the experimentally determined structures and in idealized C_{2v} or C_s geometries. In most cases the differences in the two sets of calculations are small, so except where noted in the discussion the results reported here are for the idealized geometries. The model cluster $Fe_4O(CO)_{12}$ was constructed by simply substituting O for N in the idealized $[Fe_4N(CO)_{12}]^-$ cluster. It is likely that the structure of $Fe_4O(CO)_{12}$ would be slightly different than the structure of $[Fe_4N(CO)_{12}]^-$ (cf. the differences between $[Fe_4C(CO)_{12}]^{2-}$ and $[Fe_4N(CO)_{12}]^-$), but the effects of substituting O for N should be greater than any effects caused by these small differences in structure.

All of the results described here were obtained by Fenske–Hall molecular orbital calculations.[12] The 1s through *nd* functions for Fe and Ru were taken from Richardson et al.,[13] while the $(n+1)$s and $(n+1)$p functions were chosen to have exponents of 2.0 for Fe and 2.2 for Ru. The carbon, nitrogen, and oxygen functions were taken from the double-ζ functions of Clementi.[14] The valence p functions were retained as the double-ζ functions, while all other functions were reduced to single-ζ form. In all of the calculations the local coordinate system on the carbido, nitrido, or oxido atom was oriented with the x axis parallel to a line connecting the two hinge atoms, the y axis parallel to a line connecting the two wingtip irons, and the z axis pointing out of the cluster.

Results and Discussion

Electronic Structure of $[Fe_4N(CO)_{12}]^-$ and $Fe_4O(CO)_{12}$. The calculated energy level diagrams for $[Fe_4C(CO)_{12}]^{2-}$, $[Fe_4N(CO)_{12}]^-$, and $Fe_4O(CO)_{12}$ (all having C_{2v} symmetry) are shown in Figure 1. Before making detailed comparisons of the energy levels and the bonding in the three clusters, it is useful to first review the bonding in $[Fe_4C(CO)_{12}]^{2-}$.[7] The higher energy molecular orbitals of $[Fe_4C(CO)_{12}]^{2-}$ (Figure 1a) can be divided into those that are mainly localized on the metal framework and those that represent interactions between carbon and metal orbitals. The metal-based orbitals fall into two groups. These can be described as combinations of orbitals from the four $Fe(CO)_3$ fragments making up the metal butterfly.[15] The lower energy metal orbitals are combinations of the "t_{2g}" orbitals from the $Fe(CO)_3$ groups and are nonbonding between the Fe atoms. These orbitals are indicated on the diagram as two blocks of Fe nb orbitals. The three highest energy occupied orbitals in the cluster ($3a_2$, $5b_2$, and $6a_1$) are localized on the metal framework and are derived primarily from the $Fe(CO)_3$ "e_g" orbitals. Much of the metal framework bonding occurs through these three cluster orbitals. Representations of these orbitals are shown in Figure 2.

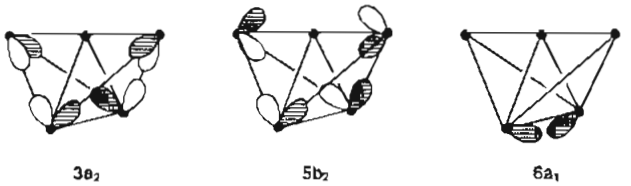

Figure 2. Schematic representations of the three highest energy occupied orbitals in $[Fe_4C(CO)_{12}]^{2-}$. These three orbitals are all bonding between the iron framework atoms.

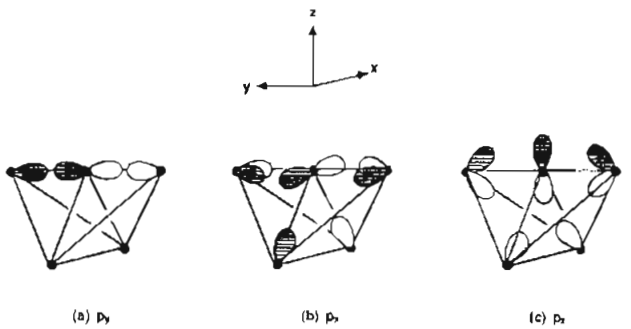

Figure 3. Schematic representations of the bonding interactions between the carbido carbon p_y (a), p_x (b), and p_z (c) orbitals and the iron framework orbitals in $[Fe_4C(CO)_{12}]^{2-}$. The local coordinate system on the carbon atom is defined as shown.

Significant metal–carbon interactions occur in the six remaining orbitals shown in Figure 1a. These six orbitals are grouped into two sets. The orbitals in the lower energy set, labeled M–C, have high carbon content and are bonding between the C 2p orbitals and both t_{2g}- and e_g-type Fe orbitals. The orbitals in the higher energy set, labeled M–C, are antibonding between the C 2p and Fe t_{2g}-type orbitals and bonding between the C 2p and Fe e_g-type orbitals. These three orbitals are centered more on the iron atoms than on the carbon, but they do have significant carbon character. Since both sets of M–C orbitals are occupied, there is no net bonding between the carbon and t_{2g}-type Fe orbitals. Thus, all of the net metal contribution to the metal–carbon bonding as well as to the metal–metal bonding comes from e_g-type Fe orbitals. The important bonding interactions between the C atom and the metal framework orbitals are illustrated in Figure 3.

The same groups of levels are found in all three level diagrams shown in Figure 1, but the relative energies of the levels having high interstitial atom character change as this atom is varied. For example, the three levels in $[Fe_4N(CO)_{12}]^-$ that have the largest N character (the levels labeled M–N in Figure 1b) lie at a lower energy, relative to the metal orbitals, than the corresponding M–C levels in $[Fe_4C(CO)_{12}]^{2-}$. This reflects the lower energy of the N atomic orbitals. Likewise, the O-based levels in $Fe_4O(CO)_{12}$ lie even lower in energy, reflecting the even lower energy of the O atomic orbitals. Only two low-energy M–O levels, those corresponding to the O $2p_x$ and $2p_z$ orbitals, are shown on the dia-

(12) Hall, M. B.; Fenske, R. F. *Inorg. Chem.* **1972**, *11*, 768.
(13) Richardson, J. W.; Nieupoort, W. C.; Powell, R. R.; Edgell, W. F. *J. Chem. Phys.* **1962**, *36*, 1057. Richardson, J. W.; Blackman, M. J.; Ranochak, J. E. *J. Chem. Phys.* **1973**, *58*, 3010.
(14) Clementi, E. *J. Chem. Phys.* **1964**, *40*, 1944.
(15) Elian, M.; Hoffmann, R. *Inorg. Chem.* **1975**, *14*, 1058.

Table V. Metal–Metal Overlap Populations

	M_h–M_h	M_w–M_h
$[Fe_4C(CO)_{12}]^{2-}$		
d–d	0.014	0.008
total M–M	0.075	0.036
$[Fe_4N(CO)_{12}]^-$		
d–d	0.016	0.008
total M–M	0.077	0.031
$Fe_4O(CO)_{12}$		
d–d	0.018	0.008
total M–M	0.077	0.028
$[Ru_4N(CO)_{12}]^-$		
d–d	0.024	0.011
total M–M	0.133	0.062

gram. There is no one orbital containing high O $2p_y$ character. Instead, $2p_y$ character is found in several lower energy orbitals that lie off the energy scale of the diagram.

The change in interstitial atom has little effect on the ordering or character of the metal-based cluster orbitals. In particular, the three highest energy orbitals are always the $6a_1$, $5b_2$, and $3a_2$ orbitals illustrated in Figure 2. The ordering and character of these levels depends on the butterfly geometry of the metal framework rather than the type of interstitial atom. It should be noted that although the $6a_1$ orbital is shown in Figure 1 as the HOMO in both $[Fe_4N(CO)_{12}]^-$ and $Fe_4O(CO)_{12}$, the $6a_1$ and $5b_2$ orbitals are nearly degenerate. Calculations for $[Fe_4N(CO)_{12}]^-$ in its real geometry show that a small distortion from the idealized C_{2v} symmetry leaves the orbitals nearly degenerate but reverses the ordering of the $6a_1$ and $5b_2$ orbitals, so it is not certain which of these orbitals is actually the HOMO. Since the calculations for $Fe_4O(CO)_{12}$ were carried out for a model cluster based upon the structure of $[Fe_4N(CO)_{12}]^-$, the three highest energy orbitals are nearly identical in the two clusters.

Changes in the electronic structure of the cluster resulting from the change in interstitial atom can be separated into those that occur within the metal framework itself or those that are associated with the interaction between the metal framework and the interstitial atom. The changes in metal–metal bonding are quite small. The metal–metal overlap populations listed in Table V indicate that the strengths of the metal–metal bonds are similar in all three clusters. In all of the clusters the overlap population between the two Fe atoms (Fe_h) making up the hinge of the butterfly framework is about twice as large as the overlap population between a hinge Fe atom and an Fe atom (Fe_w) situated at a wingtip of the butterfly framework, indicating that the Fe_h–Fe_h bond is considerably stronger than the Fe_h–Fe_w bonds. Varying the interstitial atom has almost no effect on the hinge Fe–Fe bond, but a very small decrease in the Fe_h–Fe_w overlap population is observed as C is replaced by N and O. This decrease is somewhat unexpected, since the length of the Fe_h–Fe_w bond is actually slightly shorter in $[Fe_4N(CO)_{12}]^-$ than in $[Fe_4C(CO)_{12}]^{2-}$. It appears that the small decrease in Fe_h–Fe_w overlap population is actually related to changes in the interaction between the metal framework and the interstitial atom. This will be discussed below.

Significant changes in the interactions between the interstitial atom and the metal framework are observed when the interstitial atom is varied. In $[Fe_4C(CO)_{12}]^{2-}$,[7] the C p_y orbital interacts with the wingtip irons to form a strong σ bond (Figure 3a). This is the strongest Fe–C interaction in the cluster. The C p_x and p_z orbitals interact with both the hinge and wingtip Fe atoms, forming σ bonds with the hinge atoms and π bonds with the wingtip atoms (Figure 3b,c). The relative strengths of these interactions are related to the relative sizes of the C–Fe overlap populations listed in Table VI. The combined σ and π C–Fe_w bonds result in the C–Fe_w bond being considerably stronger than the C–Fe_h bond. When either N or O replaces C in the cluster, the most significant change in bonding is the weakening of the π bonds between the interstitial atom and the wingtip Fe atoms. This reflects both the poorer overlap between the smaller N 2p orbitals (or the even smaller O 2p orbitals) and the Fe orbitals and the greater energy separation between the N or O orbitals and the Fe orbitals. In $[Fe_4N(CO)_{12}]^-$, the weaker π bonding is to some extent compensated by small increases in the strengths of the σ interactions. In $Fe_4O(CO)_{12}$, however, it is apparent that now both the σ and π interactions are weaker than in $[Fe_4N(CO)_{12}]^-$. In $[Fe_4C(CO)_{12}]^{2-}$ the total C–Fe_w overlap population is about 50% greater than the C–Fe_h overlap population, while in $[Fe_4N(CO)_{12}]^-$ and $Fe_4O(CO)_{12}$ the total X–Fe_w overlap population is only about 24% and 16% greater, respectively, than the X–Fe_h overlap population.

The X–Fe and Fe_h–Fe_w bonds are slightly shorter in the nitride than in the carbide, and it appears that in order to optimize the Fe–N bonds the N atom and the two wingtip Fe atoms all move slightly closer to the hinge Fe atoms. This shortens all of the Fe–N bonds and preserves a nearly linear Fe_w–N–Fe_w bond, thus maintaining sufficient overlap between the smaller N orbitals and the metal framework. Even with these changes in structure, however, the X–Fe_w π bonds are weaker in the nitride. In the oxide this effect is even more pronounced. As noted above, the Fe_w–Fe_h overlap populations decrease slightly from $[Fe_4C(CO)_{12}]^{2-}$ to $[Fe_4N(CO)_{12}]^-$ to $Fe_4O(CO)_{12}$, even though the Fe_w–Fe_h bonds are slightly shorter in the Fe_4N cluster. This can be related to the weaker X–Fe_w π interactions in the nitride and oxide clusters. The diagrams in Figure 3 show that in $[Fe_4C(CO)_{12}]^{2-}$ the interactions which are bonding between the C p_x and p_z orbitals and the metal framework orbitals are also weakly bonding between the hinge and wingtip Fe atoms. Although the majority of the Fe_w–Fe_h bonding occurs through the $3a_2$ and $5b_1$ orbitals (see Figure 2), the interactions depicted in Figure 3b,c do contribute to the Fe_w–Fe_h bonds. The Fe_w contribution to the interactions shown in Figure 3b,c decreases from the Fe_4C to Fe_4N to Fe_4O cluster. Consequently, the cluster orbitals involving X p_x and p_z orbitals become less bonding between the wingtip and hinge Fe atoms, and a small decrease in the Fe_h–Fe_w overlap population is observed.

In summary, the major effect of substituting N or O for C is a significant weakening of the X–Fe_w bond. This is accompanied by a small weakening of the Fe_h–Fe_w bonds. It is clear that the optimization of the cluster geometry in the butterfly clusters is a complicated process that optimizes metal–X, metal–metal, and metal–ligand bonds. The strong interactions between the interstitial atom and the metal framework are particularly important for the stability of the cluster. The existence and structure of several M_4N clusters indicate that even though N–M_w interactions are weaker in the nitride clusters than C–M_w interactions in the corresponding carbide clusters, the combined N–M and M–M bonds are sufficient to maintain nearly identical cluster configurations in the nitride and carbide clusters. The weakening of the O–Fe bonds in the Fe_4O cluster is substantial, however, and this suggests that due to the O atom's smaller size the O–Fe interactions may not be sufficient to maintain this same cluster geometry. The formation of stronger Fe–O bonds would require shorter Fe–O distances. This would in turn require all the Fe–Fe distances to shorten—a change that could be both sterically and energetically unfavorable. It is notable that although there are several complexes containing a three-coordinate pyramidal O atom,[16] the first cluster containing a four-coordinate O atom has

Table VI. X–M Overlap Populations (X = C, N, O)

	$[Fe_4C(CO)_{12}]^{2-}$		$[Fe_4N(CO)_{12}]^-$		$Fe_4O(CO)_{12}$		$[Ru_4N(CO)_{12}]^-$	
	Fe_h	Fe_w	Fe_h	Fe_w	Fe_h	Fe_w	Ru_h	Ru_w
p_x–M(d,s,p)	0.084	0.040	0.098	0.025	0.088	0.013	0.096	0.029
p_y–M(d,s,p)	0.000	0.162	−0.003	0.167	−0.005	0.155	−0.004	0.168
p_z–M(d,s,p)	0.081	0.047	0.086	0.032	0.077	0.018	0.086	0.033
total p–M(d,s,p)	0.165	0.249	0.181	0.224	0.160	0.186	0.178	0.230

Table VII. Comparisons among $[M_4N(CO)_{12}]^-$ Clusters (M = Fe, Ru, Os)[a]

	angle, deg		bond dist, Å					
	M_w–M_h–M_h–M_w	M_w–N–M_w	M_w–N (av)	M_h–N (av)	M_w–M_h (av)	M_h–M_h	M_w–M_w	ref
$[Fe_4N(CO)_{12}]^-$	101.8	179.0 (3)	1.771 (5)	1.900 (5)	2.604 (7)	2.512 (1)	3.541 (1)	10
$[Ru_4N(CO)_{12}]^-$	103.4	176.2 (2)	1.920 (3)	2.069 (3)	2.787 (9)	2.672 (1)	3.838 (1)	this work
$[Os_4N(CO)_{12}]^-$	105.4		1.96 (2)	2.12 (2)	2.808 (10)	2.728 (2)	3.903 (1)	18

[a] M_w, wingtip metal atom; M_h, hinge metal atom.

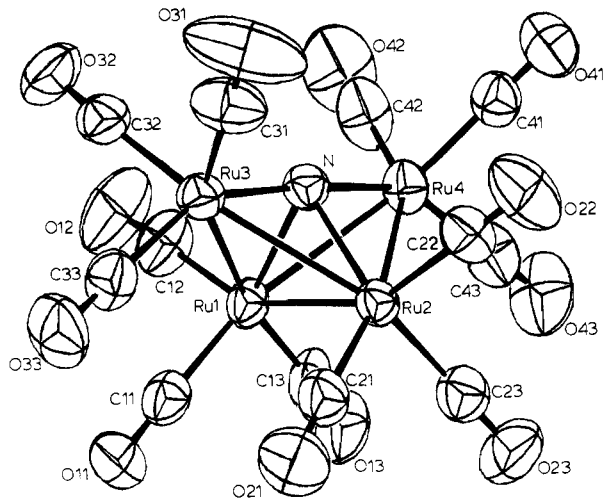

Figure 4. Structure and labeling scheme of $[Ru_4N(CO)_{12}]^-$.

only recently been reported.[3] Although this cluster, $[MnFe_3O(CO)_{12}]^-$, can be described as a butterfly oxido cluster in which the Mn atom occupies one of the wingtip positions, the structure of this cluster is considerably different from the structure of the "normal" butterfly clusters. $[MnFe_3O(CO)_{12}]^-$ exhibits an asymmetric structure with three equal length Fe–Fe bonds, and four equal length M–O bonds. The geometry of the $Fe_3(CO)_9O$ unit within the cluster is almost unchanged from that observed in $[Fe_3(CO)_9O]^{2-}$,[16a] and both the molecular and electronic structures[17] of the cluster suggest that although O is four-coordinate, the cluster is best described in terms of the triiron–O and $Mn(CO)_3$ units. Thus, even though the O atom in this cluster is four-coordinate, the geometry of the cluster is not the familiar closed butterfly found in the carbide and nitride clusters. It was previously suggested that the small size of the O atom is responsible for the preference of O for three-coordination.[2] Both the results of the calculations for $Fe_4O(CO)_{12}$ and the structure of $[MnFe_3O(CO)_{12}]^-$ tend to confirm this suggestion.

Molecular Structure of [PPN][$Ru_4N(CO)_{12}$]. The structure consists of well-separated cations and anions. The anion and labeling scheme are shown in Figure 4. Selected bond angles and distances are listed in Tables III and IV, respectively. The $[Ru_4N(CO)_{12}]^-$ anion exists in the now well-known butterfly geometry of metal atoms. Not surprisingly, it is isostructural with both $[Fe_4N(CO)_{12}]^-$[10] and $[Os_4N(CO)_{12}]^-$,[18] thus completing the homologous series. As observed in the previous nitrido cluster anions, the nitrogen atom is found in an approximately octahedral coordination geometry, with two cis sites vacant. Three terminal carbonyl ligands are bound to each metal atom, resulting in an overall C_{2v} symmetry for the anion.

A comparison of the structural features of the three nitrido anions $[M_4N(CO)_{12}]^-$ (M = Fe, Ru, Os) reveals several interesting common features (Table VII). For example, in all three clusters the nitrogen to hinge metal atom distances average 0.13–0.16 Å longer than the N–M(wingtip) distances. The metal–metal bond lengths also vary systematically; the wingtip to hinge metal atom distances average 0.1 Å longer than the bonds between the two hinge metals. Finally, as the size of the metal atom increases, the dihedral angle (M_w–M_h–M_h–M_w in Table VII) slightly increases.

Electronic Structure of $[Ru_4N(CO)_{12}]^-$. The structure determination of $[Ru_4N(CO)_{12}]^-$ makes it possible to compare two structurally similar butterfly clusters containing 3d and 4d metals. The calculated energy level diagrams for both $[Fe_4N(CO)_{12}]^-$ and $[Ru_4N(CO)_{12}]^-$ are shown in Figure 5. The energies of the metal-based $Fe(CO)_3$ and $Ru(CO)_3$ fragment orbitals are also shown in Figure 5. Although the diagrams for the two clusters are very similar, the energies of the metal-based cluster orbitals are affected by the change from Fe to Ru. In particular, the energy range spanned by the metal-based orbitals in $[Ru_4N(CO)_{12}]^-$ is greater than in $[Fe_4N(CO)_{12}]^-$. As noted above, the groupings of the metal-based orbitals in these clusters reflect the groupings of "t_{2g}"- and "e_g"-type orbitals for the $M(CO)_3$ fragments within the cluster. As might be expected, the ligand field type splitting between these "t_{2g}" and "e_g" groups of orbitals is larger for Ru than for Fe, and this larger splitting is reflected by the larger separations between the groups of metal-based orbitals in the cluster. The change from Fe to Ru has little effect on the ordering of the metal-based cluster orbitals within the various groups, however. In particular, the three highest energy orbitals are always the $6a_1$, $5b_2$, and $3a_2$ orbitals illustrated in Figure 2. The ordering of these levels depends on the butterfly geometry of the metal framework rather than on the type of metal within the framework. Just as in $[Fe_4N(CO)_{12}]^-$, the two highest energy occupied orbitals in $[Ru_4N(CO)_{12}]^-$, $6a_1$ and $5b_2$, are nearly degenerate, although the $6a_1$ orbital lies slightly higher in energy. Once again, calculations for $[Ru_4N(CO)_{12}]^-$ in its true geometry show that a small distortion from the idealized C_{2v} symmetry reverses the ordering of the $6a_1$ and $5b_2$ orbitals. Thus, in both $[Fe_4N(CO)_{12}]^-$ and $[Ru_4N(CO)_{12}]^-$ the two highest energy occupied orbitals lie very close in energy.

When Fe is replaced by Ru, changes in the electronic structure of the cluster occur primarily within the metal framework. We would expect the metal–metal bonding to be stronger between the second-row Ru atoms than between the first-row Fe atoms, and a comparison of the metal–metal overlap populations listed in Table V confirms that this is the case. The total Ru–Ru overlap populations are about twice as large as the comparable Fe–Fe overlap populations in $[Fe_4N(CO)_{12}]^{2-}$. These larger values reflect the greater overlaps and thus stronger interactions and bonds between the larger Ru orbitals. Just as in $[Fe_4N(CO)_{12}]^-$, the overlap population between the two backbone metals in $[Ru_4N(CO)_{12}]^-$ is about twice as large as that between a backbone and wingtip metal, indicating that the bond between the two backbone metals is considerably stronger than the bonds between the backbone and wingtip metal atoms. In contrast to the M–M overlap populations, the N–M overlap populations in $[Fe_4N(CO)_{12}]^-$ and $[Ru_4N(CO)_{12}]^-$ (Table VI) are almost identical. Thus, replacing Fe with Ru leads to considerably stronger metal–metal bonds but has a less significant effect on the N–M bonds. The similarities in N–M bonding suggest that, for either Fe atoms or the larger Ru atoms, the butterfly cluster structure accommodates

(16) (a) Ceriotti, A.; Resconi, L.; Demartin, F.; Longoni, G.; Manassero, M.; Sansoni, M. *J. Organomet. Chem.* **1983**, *249*, C35. (b) Uchtman, V. A.; Dahl, L. F. *J. Am. Chem. Soc.* **1969**, *91*, 3763. (c) Goudsmit, R. J.; Johnson, B. F. G.; Lewis, J.; Raithby, P. R.; Whitmire, K. H. *J. Chem. Soc., Chem. Commun.* **1983**, 246. (d) Bertolucci, A.; Freni, M.; Romiti, P.; Ciani, G.; Sironi, A.; Albano, V. G. *J. Organomet. Chem.* **1976**, *113*, C61. (e) Columbie, A.; Bonnet, J.-J.; Fompeyrine, P.; Lavigne, G.; Sunshine, S. *Organometallics* **1986**, *5*, 1154. (f) Gibson, C. P.; Huang, J.-S.; Dahl, L. F. *Organometallics* **1986**, *5*, 1676.
(17) Schauer, C. K.; Sabat, M.; Harris, S.; Shriver, D. F. Manuscript in preparation.
(18) Collins, M. A.; Johnson, B. F. G.; Lewis, J.; Mace, J.; Morris, J.; McPartlin, M.; Nelson, W. J. H.; Puga, J.; Raithby, P. R. *J. Chem. Soc., Chem. Commun.* **1983**, 689.

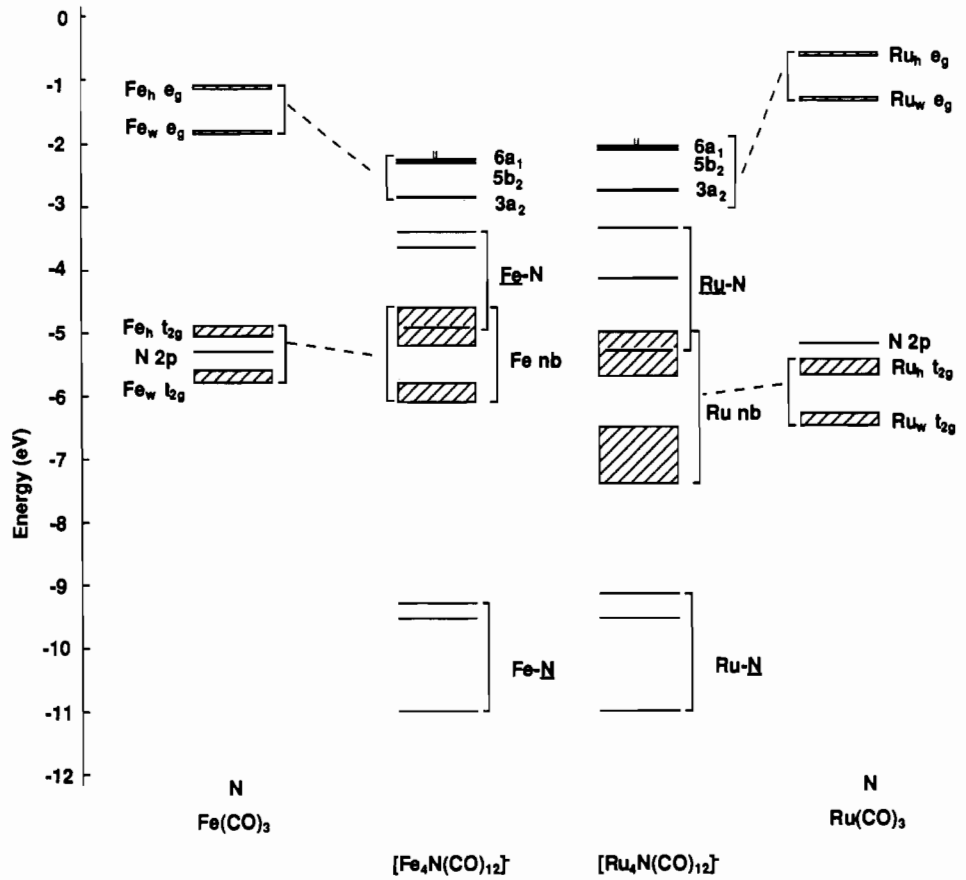

Figure 5. Calculated energy level diagrams for $[Fe_4N(CO)_{12}]^-$ and $[Ru_4N(CO)_{12}]^-$. The energies of the N 2p atomic orbitals and the metal-based $Fe(CO)_3$ and $Ru(CO)_3$ fragment orbitals are also shown on the diagram.

the N atom to form effective N–M as well as M–M bonds. It is likely that the changes in dihedral angles which are observed in the two clusters result from the optimizations of these interactions. Overall, the stronger Ru–Ru bonds suggest greater stability of the Ru_4N cluster. Given this apparent increase in stability of the Ru cluster, it is interesting to speculate about the possibility of a butterfly *oxido* cluster containing 4d rather than 3d metals. Although we would expect the O–M interactions to once again be weaker than the corresponding N–M interactions, the greater metal–metal bond strengths provided by the 4d metals might provide the stability necessary to form an M_4O cluster having a structure resembling that of the carbide and nitride butterfly clusters. The stronger M–M bonds could more than compensate for the weak O–M bonds, so that structural changes which strengthen the O–M bonds but alter the cluster framework geometry might not be necessary.

It was noted above that both the character and ordering of the frontier metal framework bonding orbitals are very similar in $[Fe_4C(CO)_{12}]^{2-}$, $[Fe_4N(CO)_{12}]^-$, and $[Ru_4N(CO)_{12}]^-$. Earlier molecular orbital calculations for $[Fe_4C(CO)_{12}]^{2-}$ showed that the reactivity of this cluster toward protonation can be related to the character of these frontier orbitals.[7] In particular, protonation of $[Fe_4C(CO)_{12}]^{2-}$ yields the hydride cluster $[HFe_4C(CO)_{12}]^-$, in which a hydrogen atom bridges the two hinge Fe atoms. A second protonation of the cluster yields the methylidyne product cluster $HFe_4(CH)(CO)_{12}$, in which the second hydrogen bridges the carbido atom and a wingtip Fe atom. The $6a_1$ HOMO in $[Fe_4C(CO)_{12}]^{2-}$ is localized across the hinge bond, and it is this orbital that interacts with a proton to give the hydride product cluster. The HOMO in $[HFe_4C(CO)_{12}]^-$ becomes the $5b_2$ orbital illustrated in Figure 2. The character of the $5b_2$ orbital suggests that reaction with a second proton involves an interaction between this orbital and the proton followed by a rearrangement of the cluster to allow bonding of the hydrogen atom to both the C and wingtip Fe atoms. The single protonation of both $[Fe_4N(CO)_{12}]^-$ and $[Ru_4N(CO)_{12}]^-$ also yields a hydride product in which the hydrogen bridges the two hinge metal atoms,[19] and we can once again associate the formation of these products with the presence of the hinge bonding $6a_1$ orbital. It should also be observed, however, that although the protonation products are similar for the carbido and nitrido clusters, the protonation reaction appears to proceed via an imido intermediate for the nitrido clusters.[19] One explanation for this reaction pathway in the nitrido cluster could involve the initial interaction between the proton and the $5b_2$ orbital of the cluster. This could be followed first by a rearrangement to give the imido (NH) intermediate (similar to the methylidyne product for the carbido cluster) and finally by the migration of the hydrogen to the hinge to yield the hydride product. The calculations presented here provide an explanation for the ultimate formation of the stable hydride product, but they do not enable us to follow the energy of possible reaction pathways or to understand what factors influence the stability of such an imido intermediate. This would require a much more extensive set of calculations.

$[FeRu_3N(CO)_{12}]^-$. This cluster exists as two isomers (I and II), with the Fe atom occupying either the wingtip or hinge position.

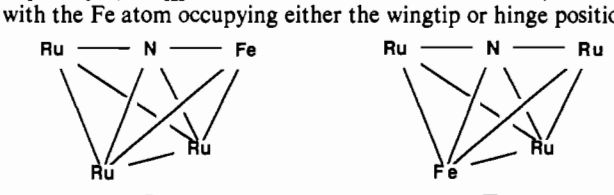

Both in the solid and in solution isomer I predominates, although in solution the two isomers are found to interconvert.[9] In other structurally characterized heterometallic butterfly carbide and nitride clusters the heterometal occupies a hinge position.[19,20]

(19) Blohm, M. L.; Fjare, D. E.; Gladfelter, W. L. *J. Am. Chem. Soc.* **1986**, *108*, 2301.
(20) Hriljac, J. A.; Swepston, P. N.; Shriver, D. F. *Organometallics* **1985**, *4*, 158.

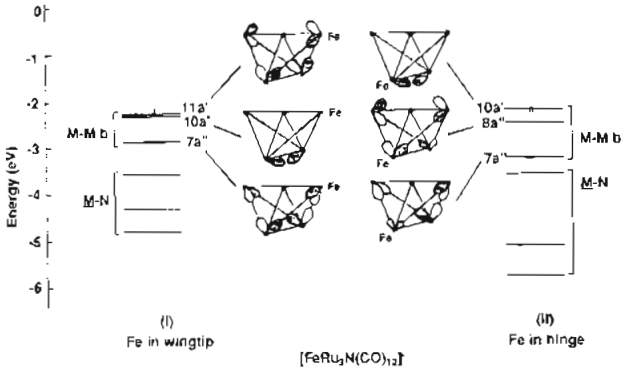

Figure 6. Calculated energies for the six highest energy occupied metal–metal and metal–nitrogen bonding orbitals in the two isomers of $[FeRu_3N(CO)_{12}]^-$. Representations of the highest energy metal framework bonding orbitals are shown in the center.

Previous molecular orbital calculations for $[RhFe_3C(CO)_{12}]^-$ and the model cluster $[MnFe_3(CO)_{13}C]^-$ showed that the metal framework bonding orbitals in these two clusters have very different character than the corresponding orbitals in $[Fe_4C(CO)_{12}]^{2-}$.[21] These differences were attributed both to the lower symmetry of the heterometallic cluster (C_s versus C_{2v}) and to the considerable separation in energy between the Rh or Mn and Fe e_g orbitals used in metal–metal bonding. In both $[FeRu_3N(CO)_{12}]^-$ clusters the symmetry is also reduced to C_s, but now even though the t_{2g}–e_g orbital splitting is larger for Ru than for Fe, the actual energies of the e_g orbitals used for metal–metal bonding are quite similar for Ru and Fe. This is considerably different from the case for $[RhFe_3C(CO)_{12}]^-$, for example, where the Rh_h e_g orbitals were calculated to lie about 1.4 eV below the Fe_h e_g orbitals. On the basis of this consideration alone, we would expect the substitution of an Fe atom into the Ru_4 framework to perturb the metal framework bonding orbitals less than the substitution of Rh into the Fe_4 framework, and this is exactly what is observed.

The calculated energies of the six highest energy occupied orbitals for both I and II are shown in Figure 6. Because both I and II have C_s symmetry, all of the cluster orbitals now have either a′ or a″ symmetry. The most significant differences in electronic structure in I and II occur in the metal framework bonding, so the discussion will focus on the orbitals associated with the metal framework. Representations of the three highest energy occupied orbitals, the metal framework bonding orbitals, are shown in the center of Figure 6. In I, where Fe occupies a wingtip position, the character of these orbitals is nearly the same as the character of the three corresponding orbitals in the homometallic clusters (Figure 2). The only significant difference between the orbitals in I and the homometallic cluster orbitals shown in Figure 2 occurs in the character of 7a″ and 11a′. In I, the Fe contribution to both of these orbitals is about 1.5 times greater than the Ru_w contribution, while in the higher symmetry homometallic clusters the wingtip atoms contribute equally to the corresponding $3a_2$ and $5b_2$ orbitals. The orbital structure is somewhat more perturbed by the substitution of an Fe atom into a hinge position. In II, the 7a″ orbital is similar to the $3a_2$ orbital in the homometallic cluster, but now it is primarily bonding between the three Ru atoms. The 8a″ orbital in II most resembles the $5b_2$ orbital in the homometallic cluster, but now this orbital is primarily bonding between the Fe and wingtip Ru atoms. The HOMO, 10a′, is very similar to the $6a_1$ hinge bonding orbital. Even though the two hinge metals are different, they make nearly equal contributions to the hinge bonding orbital. Substitution of Fe into a wingtip position thus perturbs the metal–metal bonding orbitals to a smaller degree than substitution of Fe into a hinge position. Still, the perturbation of the metal–metal bonding orbitals brought about by substitution of Fe in the hinge is less severe than that observed in $[RhFe_3C(CO)_{12}]^-$.

The character of the metal bonding orbitals in the two isomers is particularly interesting, because it has been possible in several instances to relate the structure of the protonation products in several butterfly clusters to the character of the corresponding metal bonding orbitals.[7,21] As was discussed in the previous section, addition of a proton to a homometallic carbido or nitrido cluster leads to a hydride product in which hydrogen bridges the two hinge Fe atoms. The formation of this hydride product can be associated with the very localized hinge bonding metal framework orbital ($6a_1$ in Figure 2). Addition of a proton to $[RhFe_3C(CO)_{12}]^-$, on the other hand, leads to a methylidyne product in which the hydrogen bridges the carbido carbon and a wingtip Fe atom (III).[21]

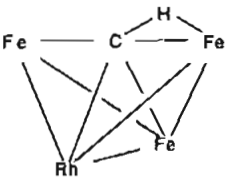

III

Molecular orbital calculations for $[RhFe_3C(CO)_{12}]^-$ showed that the character of the metal framework bonding orbitals is sufficiently perturbed by the presence of Rh in the framework that there is no very localized hinge bonding metal framework orbital. It was suggested that the absence of this type of orbital in $[RhFe_3C(CO)_{12}]^-$ is responsible for the preference for a methylidyne rather than a bridging hydride product.

The mixture of isomers I and II of $[FeRu_3N(CO)_{12}]^-$ protonates to yield one product in which the hydrogen bridges the two hinge atoms and Fe occupies exclusively a wingtip position (IV). The

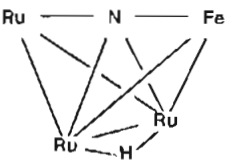

IV

calculations for the isomers I and II of $[FeRu_3N(CO)_{12}]^-$ show that a localized hinge bonding orbital is found in both isomers. It should be recognized, however, that these calculations apply to the two isomers in an idealized C_s geometry. Calculations were also carried out for the clusters in their true geometry, which is somewhat distorted from C_s symmetry. In I, where Fe occupies a wingtip position, this distortion has no effect on the character of the hinge bonding orbital. In II, however, where Fe occupies a hinge position, this distortion leads to mixing of the two highest energy orbitals 10a′ and 8a″. The two resulting orbitals now have both hinge and edge bonding character so that no one orbital is localized across the hinge. Although total energy calculations would really be necessary to compare the stability of all the possible products of protonation, these calculations suggest that the preference for the single hinge bridging product IV is related to the presence of the very localized hinge bonding orbital found in I.

It is remarkable that $[FeRu_3N(CO)_{12}]^-$ is the only heterometallic butterfly cluster for which two isomers have been isolated. In all of the characterized heterometallic carbide clusters, the heterometal occupies a hinge position. The coexistence of isomers I and II of $[FeRu_3N(CO)_{12}]^-$ indicates that the difference in energy between the two structures is rather small. Although a complete understanding of the existence or nonexistence of isomers for the various clusters would once again require total energy calculations, it is possible to make several observations that provide us with some insight into the differences between the heterometallic carbide clusters and $[FeRu_3N(CO)_{12}]^-$. First, in the heterometallic carbides, the energies of the orbitals used for metal–metal bonding are considerably different for the two metals. This leads to quite localized metal–metal bonding orbitals. In $[FeRu_3N(CO)_{12}]^-$, on the other hand, the energies of the Fe and Ru orbitals used in metal–metal bonding are nearly equal, and the comparable cluster orbitals are less perturbed (in comparison to the homometallic clusters) than the orbitals in $[RhFe_3C(CO)_{12}]^-$. Second,

(21) Hriljac, J. A.; Harris, S.; Shriver, D. F. *Inorg. Chem.* **1988**, *27*, 816.

the known carbide clusters can be viewed as derived from an Fe_4C cluster, while the heterometallic nitride cluster can be viewed as derived from an Ru_4N cluster. The metal–metal bonds in the Ru_4 framework are considerably stronger than those in the Fe_4 framework, and substitution of another metal into the Ru_4 framework could have a smaller effect on the overall stability of the metal framework than substitution of a different metal into the Fe_4 framework. Thus, when one Rh atom replaces one Fe atom in $[Fe_4C(CO)_{12}]^{2-}$, the overall perturbation of the electronic structure of the cluster is much larger than when one Fe atom replaces one Ru atom in $[Ru_4N(CO)_{12}]^-$, and it is perhaps not surprising that in the former case one isomer is strongly preferred.

Conclusions

A comparison of the electronic structures of $[Fe_4C(CO)_{12}]^{2-}$, $[Fe_4N(CO)_{12}]^-$, and $Fe_4O(CO)_{12}$ shows that the major consequence of changing the interstitial atom from carbon to nitrogen to oxygen is a significant weakening of the bonds between the interstitial atom and the wingtip metal atoms. Because of the small size of the O atom, the O–Fe interactions may not be sufficient to maintain the same butterfly cluster geometry as that observed for $[Fe_4C(CO)_{12}]^{2-}$ and $[Fe_4N(CO)_{12}]^-$. The $[Ru_4N(CO)_{12}]^-$ anion is found to be isostructural with $[Fe_4N(CO)_{12}]^-$ and $[Os_4N(CO)_{12}]^-$. The only major difference in the electronic structures of $[Fe_4N(CO)_{12}]^-$ and $[Ru_4N(CO)_{12}]^-$ is the increased strength of the metal–metal bonds in $[Ru_4N(CO)_{12}]^-$. The electronic structures of the two isomers of $[FeRu_3N(CO)_{12}]^-$ are found to be very similar. Substitution of Fe into the Ru_4 framework of $[Ru_4N(CO)_{12}]^-$ results in relatively small perturbations of the electronic structure of the cluster, and this probably accounts for the occurrence of the two isomers. Protonation of each of the nitride clusters results in a hydride cluster in which the hydrogen bridges the hinge metal atoms. In each case, this product can be associated with the presence of a high-energy cluster framework bonding orbital that is localized across the hinge of the cluster.

Acknowledgment. The portion of this research that was carried out at the University of Minnesota was supported by a grant from the National Science Foundation.

Supplementary Material Available: Lists of the temperature factors, H atom positions, and all distances and angles (12 pages); a list of the structure factors (22 pages). Ordering information is given on any current masthead page.

Contribution from the Institute for Physical and Theoretical Chemistry, University of Frankfurt, Niederurseler Hang, 6000 Frankfurt am Main, FRG, and Institute for Inorganic Chemistry, University of Witten/Herdecke, 5810 Witten, FRG

Kinetics and Mechanism of the Iron(III)-Catalyzed Autoxidation of Sulfur(IV) Oxides in Aqueous Solution. 1. Formation of Transient Iron(III)–Sulfur(IV) Complexes

Jochen Kraft and Rudi van Eldik*

Received August 3, 1988

The complex formation reactions between aquated Fe(III) and S(IV) oxides were studed spectrophotometrically (UV–vis and FT-IR) and kinetically (stopped flow) under the conditions $5 \times 10^{-4} \le$ [Fe(III)] $\le 6 \times 10^{-3}$ M, $5 \times 10^{-4} \le$ [total S(IV)] $\le 5 \times 10^{-2}$ M, $1.2 \le$ pH ≤ 3.0, $13 \le T \le 40$ °C, and 0.1 M ionic strength. Evidence is reported for the stepwise formation of 1:1, 1:2, and 1:3 sulfito complexes, depending on the pH and [total S(IV)] employed. During the first step $Fe(H_2O)_5OH^{2+}$ is rapidly substituted by HSO_3^-/SO_3^{2-} to produce a 1:1 complex ($K = 600 \pm 30$ M^{-1}), followed by a subsequent substitution at higher [total S(IV)] to produce *cis*- and *trans*-bis(sulfito) species ($K = 40 \pm 20$ and 205 ± 20 M^{-1}, respectively, at 25 °C). These species undergo a second, slower substitution reaction with rate constants of 3.3×10^3 and 4.6×10^2 M^{-1} s^{-1} (pH = 2.5), respectively, to produce a common tris(sulfito) species ($K \ge 650$ and 60 M^{-1}, respectively). The pH dependence of the reactions is accounted for in terms of various acid–base equilibria involving coordinated water and uncoordinated sulfite. The results of this study are discussed in reference to earlier studies reported in the literature.

Introduction

The mechanism of the oxidation of sulfur(IV) oxides by dissolved oxygen in aqueous solution remains unclear, notwithstanding the fact that numerous studies have been devoted to this system.[1,2] This is partly due to the fact that the reported rate laws and rate constants are inconsistent since the reaction is very sensitive to the presence of impurities, especially metal ions that can act as effective catalysts for the oxidation process.[3] In this respect it is important to note that the available kinetic data suggest that the Fe(III)-catalyzed autoxidation of S(IV) oxides can account for up to 80% of the overall oxidation rate at pH = 4–7 in aqueous solution.[2] The general interest in, and efforts to deal with, the acid rain phenomenon in recent years has encouraged us to undertake a detailed kinetic and spectroscopic study of the Fe(III)-catalyzed autoxidation of S(IV) oxides[4] as part of a broader research program dealing with metal-catalyzed atmospheric oxidation processes in general.[5] We now report our results in a series of papers dealing with the formation and decomposition reactions of Fe(III)–S(IV) transients and the overall mechanism in terms of the catalytic activity of aquated Fe(III) in the autoxidation process, respectively.[6] Mechanistic studies of the interaction of transition-metal complexes with the S(IV) oxides SO_2(aq), HSO_3^-, and SO_3^{2-} in aqueous solution have been performed by various groups,[7] especially by Harris and co-workers.[7,8] Following their[8] detailed mechanistic studies of the formation and decomposition reactions of transition-metal carbonato complexes, produced during the reaction of metal aqua species with CO_2(aq)/HCO_3^-/CO_3^{2-} (see ref 9 for a review on their work), investigations of the corresponding SO_x system were undertaken. The interactions of metal complexes with aquated CO_2 and SO_2 exhibit remarkable similarities.

In general, nonlabile octahedral metal hydroxo species can take up CO_2 and SO_2 to produce carbonato and O-bonded sulfito complexes, respectively.[10,11] The process is reversible, and on

* To whom all correspondence should be addressed at the University of Witten/Herdecke.

(1) Chang, S. G.; Littlejohn, D.; Hu, K. Y. *Science* **1987**, *237*, 756 and literature cited in ref 1 of this paper.
(2) Hoffmann, M. R.; Calvert, J. G. *Chemical Transformation Modules for Eulerian Acid Deposition Models*; Government Printing Office: Washington, DC, 1985; Vol. II (Aqueous Phase Chemistry), U.S. EPA-NCAR Interagency Agreement DW 930237.
(3) Huss, A.; Lim, P. K.; Eckert, C. A. *J. Am. Chem. Soc.* **1978**, *100*, 6252.
(4) Kraft, J. Doctoral Dissertation, University of Frankfurt, 1987.
(5) Project C3 of SFB 233 on "Dynamik und Chemie der Hydrometeore".
(6) Part 2: Kraft, J.; van Eldik, R. *Inorg. Chem.*, following paper in this issue.
(7) van Eldik, R. *Adv. Inorg. Bioinorg. Mech.* **1984**, *3*, 275 and references cited therein.
(8) Joshi, V. K.; van Eldik, R.; Harris, G. M. *Inorg. Chem.* **1986**, *25*, 2229 and references cited therein.
(9) Palmer, D. A.; van Eldik, R. *Chem. Rev.* **1983**, *83*, 651.
(10) van Eldik, R.; Harris, G. M. *Inorg. Chem.* **1980**, *19*, 880.

0020-1669/89/1328-2297$01.50/0